An Investigation of the Mechanics of Tactile Sense Using Two-Dimensional Models of the Primate Fingertip

M. A. Srinivasan

K. Dandekar

Department of Mechanical Engineering and,
Research Laboratory of Electronics,
Massachusetts Institute of Technology,
Cambridge, MA 02139

Tactile information about an object in contact with the skin surface is contained in the spatio-temporal load distribution on the skin, the corresponding stresses and strains at mechanosensitive receptor locations within the skin, and the associated pattern of electrical impulses produced by the receptor population. At present, although the responses of the receptors to known stimuli can be recorded, no experimental techniques exist to observe either the load distribution on the skin or the corresponding stress-state at the receptor locations. In this paper, the role of mechanics in the neural coding of tactile information is investigated using simple models of the primate fingertip. Four models that range in geometry from a semi-infinite medium to a cylindrical finger with a rigid bone, and composed of linear elastic media, are analyzed under plane strain conditions using the finite element method. The results show that the model geometry has a significant influence on the surface load distribution as well as the subsurface stress and strain fields for a given mechanical stimulus. The elastic medium acts like a spatial low pass filter with the property that deeper the receptor location, the more blurred the tactile information. None of the models predicted the experimentally observed surface deflection profiles under line loads as closely as a simple heterogeneous waterbed model that treated the fingerpad as a membrane enclosing an incompressible fluid (Srinivasan, 1989). This waterbed model, however, predicted a uniform state of stress inside the fingertip and thus failed to explain the spatial variations observed in the neural response. For the cylindrical model indented by rectangular gratings, the maximum compressive strain and strain energy density at typical receptor locations emerged as the two strain measures that were directly related to the electrophysiologically recorded response rate of slowly adapting type I (SAI) mechanoreceptors. Strain energy density is a better candidate to be the relevant stimulus for SAIs, since it is a scalar that is invariant with respect to receptor orientations and is a direct measure of the distortion of the receptor caused by the loads imposed on the skin.

1 Introduction

Human tactile perception is the culmination of a series of events. When the skin comes in contact with an object, mechanical loads are imposed on the skin, causing it to deform. Mechanosensitive nerve terminals distributed spatially within the skin respond with trains of electrical impulses (for a review, see Darian-Smith, 1984; Johansson and Vallbo, 1983). Four different types of mechanoreceptors and the associated afferent nerve fibers have been classified, based on their characteristic temporal pattern of impulses. When the skin is indented by a ramp-and-hold displacement of a probe, the slowly adapting type I (SAI) fibers respond to both the moving and stationary phases of the stimulus. The slowly adapting type II (SAII) fibers respond mainly to tangential skin stretch. The rapidly adapting fibers respond only when an indenting probe is moving, with type I (RAI) being most sensitive around 30 to 50 Hz vibration, and the type II (RAII) being most sensitive around 200 to 300 Hz. Thus, different receptors encode different aspects of a stimulus in terms of the frequency of impulses as a function of time and the response of all the four receptor populations taken together represents a spatiotemporal code for the applied stimulus at the skin surface. This coded information is conveyed through peripheral nerve fibers to the network of neurons in the central nervous system, where appropriate processing enables inference of the mechanical properties of objects (such as surface texture and softness) in contact and the type of contact (e.g., if the object is slipping) by touch, with or without additional information from other sensory modalities.

Clearly, the biomechanics of skin and subcutaneous tissues plays a fundamental role in the human tactile sense. It governs the mechanics of contact with the object, the transmission of the mechanical signals through the skin, and their transduction into neural signals by the mechanoreceptors. It has been hypothesized that the differences in the temporal patterns of response among the different receptor types to the same stimulus at the skin surface are due to differences in the *relevant stimulus*, i.e., a particular combination of stresses and/or strains (and their derivatives) which triggers responses in that class of receptors (Phillips and Johnson, 1981a). Further, the frequency of impulses emitted by a receptor is hypothesized to depend only on the local intensity of the relevant stimulus at the receptor site. Since the stress and strain fields sampled spatially and temporally by the receptor populations are directly dependent on the mechanical stimulus at the skin surface, these hypotheses offer a mechanism for the neural coding of tactile information about the object and the type of contact.

At present, the relevant stimulus for each mechanoreceptor type is largely unknown and its determination is an important

Contributed by the Bioengineering Division for publication in the JOURNAL OF BIOMECHANICAL ENGINEERING. Manuscript received by the Bioengineering Division April 24, 1993, revised manuscript received January 4, 1995. Associate Technical Editor: A. Erdman.

area of research on tactile sense. Although electrophysiological recordings of the neural signals transmitted by a single peripheral nerve fiber are possible in either a monkey or a human, the stress or strain state of the associated mechanoreceptors is not empirically observable at present. Therefore, mechanistic models of the skin and subcutaneous tissues are needed not only to generate hypotheses concerning the relevant stimuli for each class of receptors, but also to design the biomechanical, neurophysiological, and perceptual experiments that investigate the tactile sensory system.

The focus in this paper is the primate fingertip (distal phalanx), due to its predominant use during manual exploration and manipulation, as well as the availability of biomechanical and neurophysiological data for model verification. In the subsequent sections, several simplified models of the fingerpad are analyzed in order (1) to determine which model best matches the empirical data on skin surface deflection under a line load and (2) to hypothesize candidate relevant stimuli for SAI, based on matches between various strain measures and previously recorded neurophysiological data. In Section 2, broad issues concerning modeling the fingertip are discussed and the particular approach followed in this paper is justified. Four finite element models of the fingerpad are described in Section 3. Results of the mechanistic analyses of these models and their relationship to biomechanical and neurophysiological data are discussed in Section 4. For the analysis, indentations by line loads, rectangular bars, and gratings were chosen since experimental data was available for these loadings. Conclusions concerning the effect of model geometry on surface deflection profile, subsurface stress and strain fields, and relevant stimulus for SAI are given in Section 5.

2 Issues in Modeling the Fingertip

The structure of the primate fingertip is complex: from a macroscopic viewpoint, it mainly consists of two layers of skin, the epidermis and the dermis, which enclose subcutaneous tissues mostly composed of fat in a semi-liquid state together with a relatively rigid bone. When viewed as a block of material, it exhibits complex mechanical behavior such as nonlinear force-displacement relationship under indenting probes, anisotropy, and rate and time dependence. Quantitative data on the external and internal geometries of a typical fingertip, as well as the constitutive relations for the materials that make up the fingertip are unavailable at present. Although some data on the in vitro and in vivo mechanical properties of the skin are available (for a review, see Cook, 1975; Thacker, 1976; Fung, 1981; Lanir, 1987; Lanir et al., 1990), they have not been measured for the fingertip skin and are inappropriate for the whole primate fingertip, of which skin is one part. Furthermore, the constitutive equations and the models (for example, Danielson, 1973) that have been proposed contain a number of unknown material parameters.

At present and for the foreseeable future, a detailed model of the fingertip will have a large number of unknown geometrical and material parameters for various layers of skin and subcutaneous tissues. If they are treated as free parameters whose values are chosen such that predictions of the model match data from biomechanical and neurophysiological experiments, then the modeling process is essentially an elaborate curve-fitting procedure that does not provide any insight into the mechanistic basis of tactile sense. Alternatively, if the parameter values are arbitrarily assigned, it becomes impossible to determine the causes of success or failure of the model in explaining empirical data and to develop a constructive procedure to improve the model. In either case, the resulting model will have too many parameters compared to the empirical data it is supposed to match or predict, while at the same time is a much simplified representation of the actual geometry and material behavior of the fingertip.

To overcome the limitations arising out of a lack of experimental data and complexity of the system, a combination of mechanistic and systems modeling can be employed. In this approach, the fingerpad with all its complexity is treated as an unknown *black box*, and the goal is to develop a *reduced order* mechanistic model that matches the empirically observed input-output relationship, without attempting to model the microscopic details of the system. The strategy here is to develop a sequence of models starting with the simplest mathematically tractable model containing a minimum number of parameters and gradually approach the actual physical structure of the primate fingerpad. This sequence is guided by agreements as well as mismatches between the model predictions and the results of biomechanical and neurophysiological experiments. The hope is that a synergistic evolution of both the models and the experiments, with each feeding information to the other, will eventually result in a fully tested realistic model and a deep understanding of the neural coding of tactile information. The work presented in this paper is an initial contribution towards this goal. It should be noted that such a systems approach can be employed for mechanistic modeling of robotic tactile systems which consist of mechanoreceptors embedded in a compliant medium. The approach, however, is not limited to the analysis of tactile sensing systems, and is applicable in understanding the mechanics of any biological materials or organs.

One possible criticism of this approach in the context of tactile neural coding might be that conclusions based on simplified models are invalid in explaining experimental data from the real fingerpad. There are several responses to this criticism. First, as stated above, even detailed models of the fingerpad that take into account several layers of skin and subcutaneous tissues are quite simplistic relative to the actual biological structures. In addition, they have the problem of large number of unknown parameters. Second, a model need not and should not incorporate complexity unless it is forced to do so. Implicit in the above criticism is the assumption that the detailed geometry and material properties are of importance, which needs to be proven. For example, in the eye, although the cornea, lens, and vitreous body are structurally heterogeneous (both macro- and microscopically), they behave in concert like a simple, homogeneous lens. Radically simplified models of the cochlea have been able to explain human auditory signal processing in the periphery (Lighthill, 1991). Similarly, it needs to be examined (as is done in this paper) if the combined mechanical properties of the fingerpad and their effect on cutaneous mechanoreceptor response are simpler than that suggested by the structure of the fingerpad. Third, there are strong indications for the success of the systems approach outlined above, based on the results from extremely idealized models described below.

In order to identify the relevant stimulus of SAI mechanoreceptors (Merkel Cells), Phillips and Johnson (1981a; 1981b) recorded the responses of mechanoreceptors innervating the monkey fingerpad to steady indentations by gratings with rectangular bars. To calculate the stress and strain values at typical receptor sites within the skin, they assumed the fingertip to be mechanically equivalent to a homogeneous, isotropic, incompressible and linearly elastic half-space in a state of plane stress or strain with infinitesimal deformations. In spite of such broad idealizations, maximum compressive strain profiles calculated by the models were in excellent agreement with the recorded SAI response profiles under a range of periodic and aperiodic gratings. An alternative idealization was successful in matching the measured in vivo skin surface deflection profiles of both monkey and human fingerpads under line loads (Srinivasan, 1989). Whereas the elastic half-space model only roughly approximated the profiles, a model of the fingertip as an elastic membrane (representing the skin) enclosing an incompressible fluid (representing the subcutaneous tissues) predicted the observed surface profiles quite accurately. This "waterbed" model, however, failed to match the variations in the responses

of the receptors at different locations in the skin, owing to the uniform tension in the membrane and uniform pressure field within the fluid. If the receptors were embedded in the fluid or the membrane, all the receptors would experience the same stress state and would convey no information to infer the location of the load on the surface. Thus, the waterbed model was better for matching the available biomechanical data and the elastic half-space model was better for matching receptor response profiles.

Could it be that by employing models of about the same size and shape as the primate fingerpads, one can match both biomechanical and neurophysiological data? This is one of the primary motivations for the models presented in this paper. Such models would also remove some of the other limitations of the half-space model. For example, because the half-space surface is flat and of infinite extent, all the bars in a grating contact it simultaneously, as opposed to only a few bars contacting the small monkey fingerpad. Hence, in the half-space model, there is no distinction between the response of a population of receptors to a single indentation of the grating and the spatial response profile (see Section 4.3.1 and Fig. 7) of a single receptor to a sequence of indentations where the grating is stepped across the surface. In addition, there is no distinction between the predicted spatial response profiles of a receptor at the center of the fingerpad and one that is closer to the fingernail.

3 The Models

The uniform cross-sections of a sequence of four models composed of isotropic, incompressible, and linear elastic media are as shown in Fig. 1. Loading is confined to indentations by line loads and long bars that have been used as stimuli in previous biomechanical and neurophysiological experiments, and therefore plane strain approximations are valid in the analyses of these models. Since the loads are static and the recorded receptor responses that need to be correlated with the stress or strain measures are generally steady, the viscoelastic behavior of the fingerpad is not taken into account for this initial analysis.

The availability of analytical solutions to a line load acting upon a semi-infinite linear elastic medium (attributed to Boussinesq (1885) in Timoshenko and Goodier (1982)) provides a means of verifying the finite element calculations. This solution was also the basis of calculations done by Phillips and Johnson (1981b) in their half-space model of the monkey fingertip. Therefore, a model with a large rectangular cross-section was analyzed first and the numerical solution was compared with the analytical solution. Model dimensions of 40 mm × 18 mm containing 8-noded plane strain isoparametric elements were sufficient to match the analytical results in the region of interest (ref. Section 4). The next step was to remove the assumption of semi-infiniteness and model the finger as a finite medium. The second model was of square cross-section (8 mm × 8 mm), with dimensions comparable to the actual monkey fingerpad. To account for the effects of curvature of the central cylindrical region of typical monkey fingertips (distal phalanx), the next refinement was to model the fingertip as a cylinder of 8 mm diameter, with and without a central rigid bone of 2 mm diameter. To simulate the fingernail which is very stiff relative to the soft tissues, all the degrees of freedom were suppressed at the nodes spanning the bottom boundary of the finite square model, and a third of the boundary at the bottom of the cylindrical models.

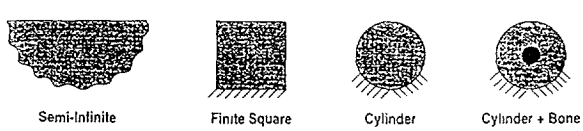

Fig. 1 Cross-sections of each of the four models composed of an incompressible elastic material and assumed to satisfy plane strain conditions. (*a*) Semi-infinite medium, (*b*) finite square (8 mm × 8 mm) (*c*) homogeneous cylinder (8 mm diameter) (*d*) cylinder (8 mm diameter) with a central rigid bone (2 mm diameter).

In the monkey fingerpad skin, Merkel cell receptors associated with SAI fibers are embedded at a depth of about 0.5 mm to 1.0 mm from the surface and the receptor spacing is of the order of 1.0 mm. In order to have sufficient spatial resolution in calculating strains at typical receptor locations, square elements of 0.125 mm sides in the top 1.0 mm thick layer of each model and 3 × 3 integration points within each element were used, resulting in an effective spatial resolution of about 0.05 mm in this region. The element size was gradually increased for deeper locations from the top surface as shown in Fig. 2. This helped to reduce the size of the problem, thereby reducing the computational effort. The aspect ratio of the elements was maintained as close to 1.0 as possible by using layers of transition elements.

For this first analysis, the material was assumed to be linear elastic and isotropic, which required the specification of only the Young's modulus and the Poisson's ratio. If the prescribed loading and boundary conditions are in terms of displacements, it can be shown that for a homogeneous model under infinitesimal deformations, the strains are independent of the Young's modulus (see Appendix). Thus, no specific value of the Young's modulus was assumed in the calculations. In vivo measurements of changes in the human fingerpad volume under indentation stimuli show that the changes are at most 5 percent (Srinivasan, et al., 1992). Therefore, to a first approximation, the fingertip can be considered to be incompressible (i.e., Poisson's ratio = 0.5). Finite element models of incompressible materials in plane strain require special care in the formulation. The mixed displacement-pressure (u-p) formulation which treats pressure as an independent nodal variable in addition to the displacements (Sussman and Bathe, 1987) was used and a Poisson's ratio of 0.48 was chosen. A subsequent analysis of some of the cases were done using a hybrid formulation which allowed the Poisson's ratio to be as high as 0.499, but no significant differences were found in the results.

The ADINA finite element software together with custom written codes for preprocessing and generating the elements was used. The cylindrical model had 856 plane strain isoparametric elements and 2633 nodes. The resulting stiffness matrix had 838,200 elements and had a mean half-bandwidth of 161. The solution time on the DEC3100 was about 140 seconds excluding pre-processing and post-processing. The same problem could be solved in about 12 seconds on the MIT CRAY-XMP. The semi-infinite model had 3190 elements and 10,859 nodes. It was necessary to solve about 150 static problems to simulate the experiment (see Fig. 7) reported by Phillips and Johnson (1981a). Depending on the model size and the computational effort involved in the simulation, either a DEC3100 workstation or the MIT CRAY X-MP supercomputer was used.

4 Results

4.1 Line Load. The surface deflection of the fingerpad under a known loading provides a clue to infer the mechanical nature of its constituent materials. Therefore the experimentally observed surface deflection profiles of monkey and human fingerpads under 1 mm indentation by a single line load were compared with the corresponding predictions of each of the models. As explained earlier and shown in Fig. 3, the Boussinesq solution does not match the experimental data points, whereas the waterbed model does predict the observed profile quite well. It should be noted that both of these analytical solutions have as a free parameter the horizontal distance from the load to the point where the deformed surface profile crosses the undeformed profile. In Fig. 3, this distance has been chosen for both the models to be the same as the one observed in the experiments. Also shown in the figure are the profiles predicted

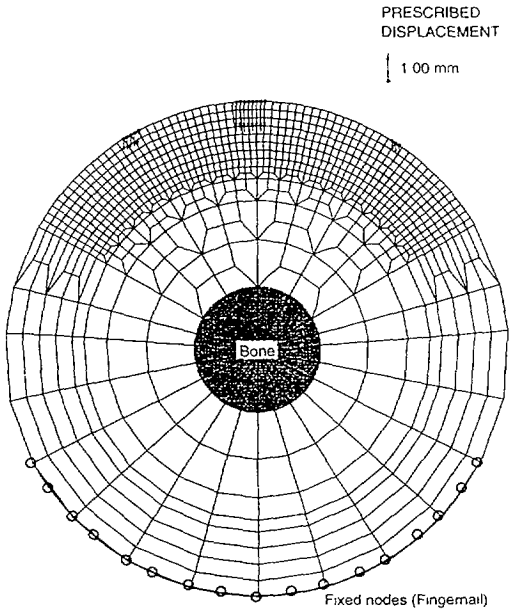

Fig. 2 Cross-section of the cylindrical model with bone is shown. The nodes on the lower third of the circumference are constrained to simulate a concentric fingernail of anatomically correct dimensions, which is modeled to be rigid relative to the soft tissues. Displacements can be prescribed on the top surface as shown. The top layer of the skin has a large number of elements where finer spatial resolution is sought. The element size is increased away from the top to reduce the computational effort.

by the four finite element models. In each of these profiles, the kink observed near the load is a numerical artifact and should be ignored. It occurred closer to the load as the element size was reduced and is due the singular nature of the concentrated load coupled with the plane strain and small deformation assumptions. An appropriate choice of the free parameter in the Boussinesq solution, different from the one shown in Fig. 3, matched the analytical and numerical profiles for the semi-infinite medium quite well. It can be seen that the profiles for the semi-infinite and finite square models are close together, as are those for the cylinder with and without the bone. If the vertical deflection, say at 2 mm from the load, is taken as a measure of the overall stiffness of the models, then the four finite element models in increasing order of stiffness are the finite square, semi-infinite, cylinder and cylinder with bone. It is clear from Fig. 3 that, irrespective of their shape, the models composed of homogeneous linear elastic medium do not predict the experimental profile as accurately as the inhomogeneous waterbed model.

Since the emission of neural impulses by the receptors is due to the opening of ionic channels caused by mechanical strains, the state of strain at receptor locations is important in predicting the receptor response. Shown in Fig. 4 are three possible candidates for the relevant stimulus to SAI. They have been calculated using the cylindrical model with bone subjected to a single line load imposed on the surface at the horizontal location 0.0. Each strain measure is evaluated at three depths in the region where the receptors are known to be located. For each of the components, the deeper the location, the more blurred is the spatial distribution. This illustrates the spatial low-pass filtering of the mechanical signals by the elastic medium and shows that the quality of information about the spatial variation of the surface stimulus decreases with increases in the depth of receptor locations.

For a given receptor depth, the degree of blurring of the strain energy density distribution is less than that of the maximum compressive strain. This is to be expected since, for the plane strain models composed of an incompressible material, it can be shown that the strain energy density is proportional to the square of the magnitude of maximum compressive strain (Ugural and Fenster, 1981). Therefore, for a given stimulus force distribution acting on the skin surface and receptor locations within the skin, the contrast in the neural code based on strain energy density is much higher than that based on maximum compressive strain. The distinct differences in the three component distributions indicates that if a fine enough probe (say, 0.2 mm dia.) is used in neurophysiological experiments,

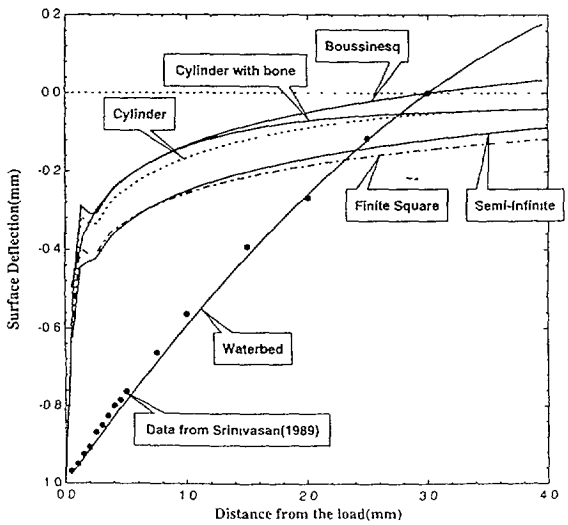

Fig. 3 Deflection profiles of the skin surface under a line load perpendicular to the model cross-sections shown in Fig. 1. Only half the profiles are shown due to symmetry. The experimental data points are the averages of the corresponding points on the left and the right side of a sharp wedge indenting a monkey fingerpad (Srinivasan, 1989). Calculated profiles are shown as continuous traces since the data points are only 0.05 mm apart.

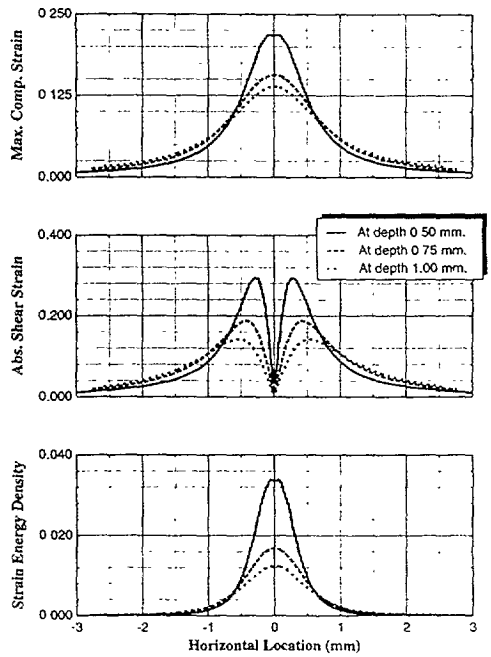

Fig. 4 Spatial distribution of subsurface strain measures under a line load applied normally to the cylinder model surface at the horizontal location 0.0. Distributions are calculated at three possible depths from the surface in the region where mechanoreceptors are typically located. As in Fig. 3, calculated profiles are shown as continuous traces since the data points are only 0.05 mm apart.

the spatial response profiles of the SAI and RAI fibers might enable the determination of their respective relevant stimuli. It should be noted that the stresses corresponding to the strain measures shown here are similar in form. The rest of the stress and strain components have not been shown due to lack of space as well as the lack of their promise as relevant stimuli for the receptor response. For the three other models described in this paper, although the magnitudes of the stress and strain state at a given location are different for a given line load, the general spatial profile of each component is approximately the same as the corresponding one for the cylinder.

4.2 Rectangular Bar. A question of considerable interest is the effect of model geometry on strains at receptor locations which, in turn, are related to neural response. The results for the four models indented to a depth of 1 mm by a 1.5 mm wide rectangular bar are shown in Fig. 5. For each model, the intensity of the surface pressure is very high under the edge of the bar relative to the pressure at the center of the bar. The spatial distribution of the three strain measures shown are essentially low-pass filtered versions of the surface pressure distribution. The extent of the filtering depends on the model as well as the particular strain measure. For example, among the models, all the strain measures for the finite square case have superior contrast between the edges and the center of the bar, and the absolute shear strain has the best contrast among the strain measures for each model. Therefore, if a robot tactile sensing system needs to be designed to detect edges, the models predict that the best performance would be achieved by shear strain sensors.

4.3 Aperiodic Grating. Neurophysiological experiments probing the primate tactile sensing system typically consist of recording the response of one peripheral nerve fiber at a time, but the responses from the population of receptors activated by a stimulus are needed to decipher the neural code for that stimulus. By carefully designing the sequential stepping of rectangular gratings across a fiber's most sensitive spot on the skin surface, Phillips and Johnson (1981a) succeeded in reconstructing a hypothetical population response from the response of a single fiber. The models described in this paper, however, are not subject to such experimental limitations and are able to simulate the mechanistic aspects of both the population response for a single stimulus or the response of a single fiber to multiple stimuli. Simulations of the sequential indentations of the cylindrical model with bone by two of the gratings used by Phillips and Johnson (1981a) were carried out and the spatial sub-surface strain distributions for each indentation of the gratings were calculated. Figure 6 shows the results of one indentation to a depth of 1 mm into the skin with an aperiodic grating composed of 1.5 mm wide bars. The spatial variation of the surface load, maximum compressive strain, shear strain, and strain energy density at a depth of 0.75 mm, which corresponds to the typical Merkel cell receptor locations in primates, are shown in the figure. Only a few bars are in contact with the cylindrical finger during any one indentation, as contrasted with contact with all the bars in the case of the semi-infinite model. Owing to the surface curvature and finite extent of the cylindrical model, the loads imposed on the model and consequently the spatial distribution of various strain measures caused by an indentation of a grating are significantly different from those predicted by the semi-infinite model used by Phillips and Johnson (1981b).

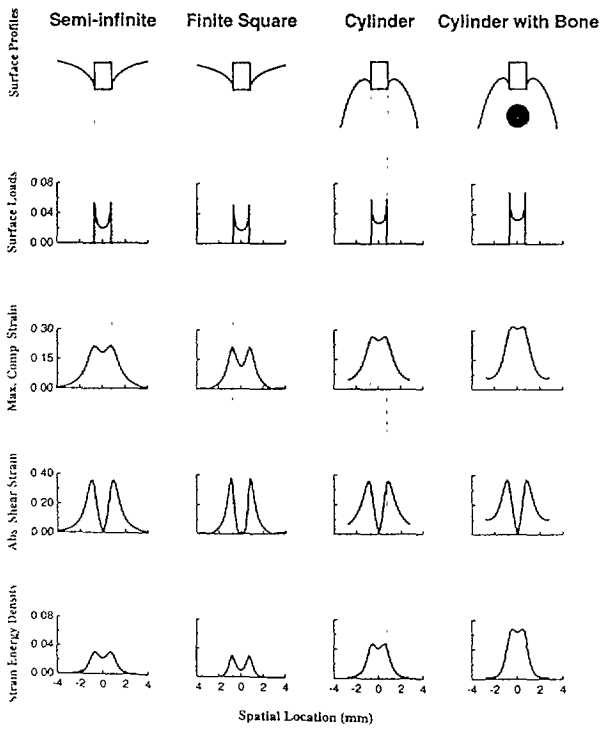

Fig. 5 Vertical indentation of each model by a 1.5 mm wide rectangular bar to a depth of 1 mm. Calculated spatial distributions of surface deflection and surface loads, as well as maximum compressive strain, absolute value of shear strain, and strain energy density at 0.75 mm depth are shown.

4.3.1 Comparison With Neurophysiological Data. In order to identify the relevant stimulus (i.e., the strain component or combination at a receptor location that is coded into neural response) for the SAIs, simulations of the stepping of aperiodic gratings across the fingerpad as done by Phillips and Johnson (1981a; 1981b) were carried out on the cylindrical model with bone. This was accomplished by performing finite element analysis of each indentation of a grating (as in Figure 6) in a sequence of about 150 indentations, where position of the grating relative to the fingerpad was shifted laterally by 0.2 mm for successive indentations. A strain measure of interest (e.g., maximum compressive strain) at a fixed receptor location within the fingerpad was extracted from the calculations for each indentation and plotted as a function of the horizontal location of the receptor relative to a fixed point on the grating. Such *spatial profiles* of maximum compressive strain, absolute shear strain, and strain energy density are shown in Figure 7 for a receptor located on the central longitudinal section of the model at 0.75 mm depth from the skin surface. The *spatial response profile* of an SAI from the experiments of Phillips and Johnson (1981a) is superimposed on each of the strain profiles for comparison.

It can be observed from Fig. 7 that the calculated strains at a fixed location under an individual bar of the grating depend on the spacing of the neighboring bars when two or more bars are in contact with the fingerpad. The finite element calculations predict almost identical strain states under each of the three rightmost bars. When the gaps are less than 1.5 mm, the strain state of the receptor is influenced by the contacting bars neighboring the one directly above the receptor.

In spite of drastic differences in the geometry and resulting strain distributions under a single indentation by a grating (Fig. 6) among the cylindrical and semi-infinite models, the calculated spatial profiles shown in Fig. 7 are surprisingly similar to those obtained by Phillips and Johnson (1981b) This is because the influence of a load on the strain state at the receptor location decreases rapidly (exponentially in the semi-infinite model) with increases in the distance between the receptor and the load. Only loads acting within a "region of influence" (which depends on the strain measure of interest, but is about the same for the two models) have a significant effect. Therefore, although the calculated strain fields and, hence, the predicted population responses are very different for cylindrical and semi-

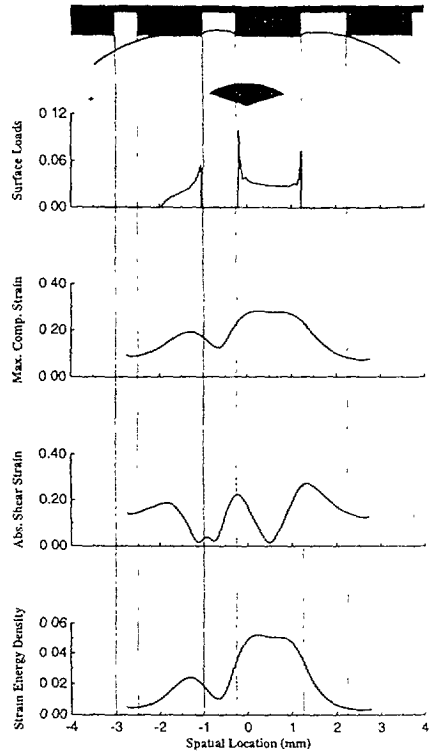

Fig. 6 Indentation of the cylindrical model with bone by an aperiodic grating with 1.5 mm bars. Shown at the top is the deformed surface of the cylinder cross-section under the grating. A portion of the bone is shown shaded. The spatial distributions of surface loads, maximum compressive strain, absolute shear strain, and strain energy density at a depth of 0.75 mm from the surface are shown.

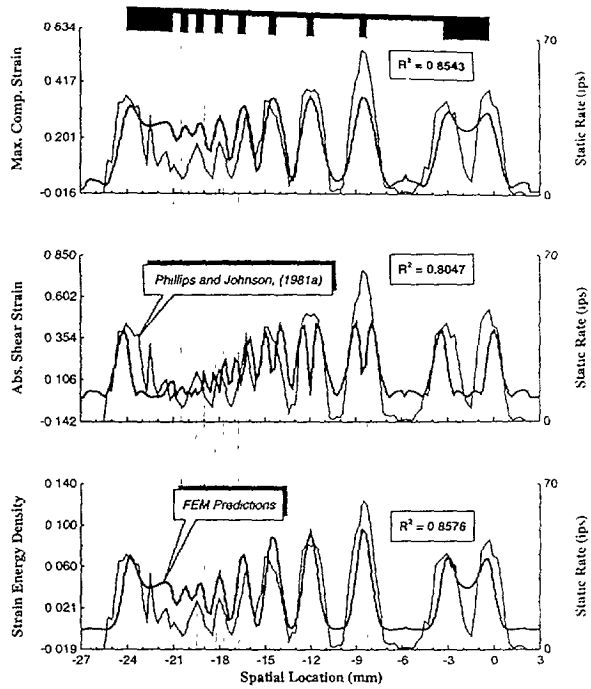

Fig. 7 Comparison of experimentally recorded SA fiber spatial response profile (Phillips and Johnson, 1981a) with spatial profiles of maximum compressive strain, absolute shear strain, and strain energy density calculated using the cylindrical model with bone. The stimulus is an aperiodic grating with 0.5 mm wide bars. The model predictions are shown as thicker traces superimposed on the experimentally recorded receptor response rate profile.

infinite models, the spatial profiles of a strain measure for the two models are similar at a central receptor location. However, the farther a receptor is from the central longitudinal section, the higher is the difference between the spatial profiles predicted by the two models.

Spatial profiles of the strain measures were compared with the experimentally observed SAI spatial response profiles. In order to correlate the two, a linear relationship between the neural discharge rate and the strain measures was assumed (Phillips and Johnson, 1981b). It was of the form,

$$d_i = a\epsilon_i + b$$

where,

d_i is the experimentally recorded response at spatial location i, and

ϵ_i is the calculated strain measure at spatial location i.

The constants a and b were determined by maximizing the goodness of fit measured as the variance ratio R^2.

$$R^2 = \frac{\Sigma d_i^2 - \Sigma e_i^2}{\Sigma d_i^2}$$

where,

e_i is the difference in the experimentally recorded response and the calculated strain measure at location i.

An R^2 value of 1.0 indicates an perfect match in the experimental data and model predictions. After investigating the goodness of fit for all the horizontal and vertical strain components, principal stresses and strains, and strain energy density for gratings with 0.5 mm and 1.5 mm bars at typical receptor locations (depths of 0.5, 0.75, and 1.0 mm from the surface), it was found that maximum compressive strain magnitude and strain energy density matched the neural data the best (R^2 = 0.8543 and 0.8576, respectively, at a depth of 0.75 mm for grating with 0.5 mm bars) and are, therefore, the top candidates for being the relevant stimulus for SAIs. A sample of results from curve fitting are shown in Table 1 for grating with 0.5 mm bars and at a depth of 0.75 mm. As noted before, for the plane strain models composed of an incompressible material, it can be shown that the strain energy density is proportional to the square of the magnitude of maximum compressive strain. Based on their semi-infinite model of the fingerpad, Phillips and Johnson (1981b) also proposed maximum compressive strain magnitude as the relevant stimulus for slowly adapting receptors. It is of interest to note that Grigg and Hoffman (1984) in their study of Ruffini mechanoreceptors in the joint capsules concluded that the strain energy density had a high correlation with the receptor response.

Table 1 Goodness of fit for various strain measures at a depth of 0.75 mm from the surface for grating with 0.5 mm wide bars. The R^2 values along with the corresponding scale and offset values are tabulated

Strain measure	R^2	a (Scale)	b (Offset)
Lateral stress	0.77	94.59	9.76
Horizontal stress	0.68	44.07	20.06
Vertical stress	0.77	51.21	10.39
Shear stress	0 80	209.03	10.00
Horizontal strain	0 77	−70.82	12.76
Vertical strain	0.77	70.72	11 81
Shear strain	0.80	70.62	10.00
Max. principal stress	0.81	63.65	5.67
Min. principal stress	0.69	−91.56	22.85
Max. principal strain	0.85	107.66	1.72
Strain energy density	0.86	219.96	8 42

Although maximum compressive strain and strain energy density have a simple nonlinear relationship for the model considered here, there are inherent differences between them which affect their suitability as relevant stimuli. If it is assumed that a particular receptor is able to measure strain in a fixed direction, then, in order to measure the maximum compressive strain at a point, the receptor should be oriented to measure strain in the principal direction. However, the principal direction at a given location varies with the stimulus, and hence a receptor fixed in location and oriented in a particular direction cannot measure the maximum compressive strain for all the stimuli. If, on the other hand, it is assumed that receptors can measure maximum compressive strain at a certain location irrespective of their own fixed orientation, then what is being postulated is, in effect, an internal information processing mechanism that picks the maximum strain among the strains in all directions. There is no evidence at present for such a mechanism to operate within a receptor or even among the complex Merkel cells believed to be the endings of SAI fibers. In contrast to the maximum compressive strain, strain energy density is an invariant of the strain tensor that does not depend on the direction of measurement at a given point and, hence, is a natural candidate to be the relevant stimulus. In addition, this scalar quantity is a measure of the amount of distortion at that location and, therefore, is possibly related directly to the opening or closing of ionic channels in the receptor. If the Merkel cell receptors generate a neural impulse rate proportional to the strain energy density in their neighborhood, then the receptors can have a fixed location and orientation relative to the skin surface and yet code with high fidelity the different mechanical stimuli imposed on the skin surface.

5 Conclusions

Understanding the mechanisms by which human sense of touch operates requires a study of the mechanics of skin and subcutaneous tissues. In this paper, a sequence of mechanistic models of the primate fingertip under plane strain conditions have been analyzed using the finite element method. It is shown that in spite of radical differences in model geometry, surface deflection profiles of models containing homogeneous linear elastic media do not match the experimentally observed ones under line loads. In contrast, the deflection profiles of the inhomogeneous "waterbed" model has been seen to match the empirical data very well (Srinivasan, 1989). It failed to match the spatial response profiles of the receptors, however, owing to the uniform pressure field within the fluid and a constant uniform tensile force in the membrane. Therefore, even though the waterbed model matches the surface deflections very well, it cannot be used to explain the transduction of mechanical stimuli into neural codes.

In the homogeneous models, the spatial distribution of the subsurface stress or strain measures are blurred versions of the surface pressure distributions, due to the low-pass filtering of mechanical signals by the elastic medium. The degree of filtering depends on both the model geometry and the particular measure of interest. The matching of the experimentally recorded spatial response profiles of receptors and the corresponding subsurface strain measures at receptor locations provides a means by which the relevant mechanical signal transduced by each class of mechanoreceptors can be inferred. Both the magnitude of maximum compressive strain and strain energy density at receptor locations emerge as strong contenders to be the relevant stimulus for SAIs. Since strain energy density is a scalar measure of distortion that is invariant with respect to receptor orientation, it is a better candidate for being the relevant stimulus. It is likely that, to match both the surface deflection and receptor response profiles, a thick elastic layer with embedded receptors and supported by an incompressible fluid or a soft solid is needed.

Acknowledgments

The work reported in this paper was supported by the NIDCD award R29-DC00625 and ONR grant N00014-92-J-1814. The authors wish to thank Prof. K. O. Johnson for making the neurophysiological data available and the anonymous reviewer who helped to improve the clarity of the paper.

APPENDIX

Strain Calculations for Finite Element Models With Prescribed Displacements

The finite element formulation for the static case reduces to

$$\mathbf{KU} = \mathbf{R}$$

where

$\mathbf{K}$ is the stiffness matrix,
$\mathbf{U}$ is the displacement vector,
$\mathbf{R}$ is the load vector.

Loads and displacements can be prescribed at any node in the model, but both displacement and forces cannot be prescribed at the same node. Thus, we can separate the total number of nodes into two sets—one that has forces prescribed and the other which has displacements prescribed. Let $\mathbf{R}_a$ be the prescribed forces and $\mathbf{U}_a$ the corresponding unknown displacements and let $\mathbf{U}_b$ be the prescribed displacements and $\mathbf{R}_b$ the corresponding unknown reaction forces. The finite element equation can be rewritten in terms of the two sets of nodes as follows:

$$\begin{bmatrix} \mathbf{K}_{aa} & \mathbf{K}_{ab} \\ \mathbf{K}_{ba} & \mathbf{K}_{bb} \end{bmatrix} \begin{Bmatrix} \mathbf{U}_a \\ \mathbf{U}_b \end{Bmatrix} = \begin{Bmatrix} \mathbf{R}_a \\ \mathbf{R}_b \end{Bmatrix}$$

The problem now reduces to finding the unknown displacements $\mathbf{U}_a$ which can be used to determine the unknown reaction forces $\mathbf{R}_b$. Rewriting, we have:

$$\mathbf{K}_{aa}\mathbf{U}_a = \mathbf{R}_a - \mathbf{K}_{ab}\mathbf{U}_b$$

$$\mathbf{R}_b = \mathbf{K}_{ba}\mathbf{U}_a + \mathbf{K}_{bb}\mathbf{U}_b$$

In the problems we have attempted, the loading is defined only by prescribing displacements and no forces are prescribed. Thus, $\mathbf{R}_a = \mathbf{0}$ and the first equation above reduces to

$$\mathbf{K}_{aa}\mathbf{U}_a = -\mathbf{K}_{ab}\mathbf{U}_b \tag{1}$$

The generic stiffness matrix is defined as

$$\mathbf{K} = \mathbf{B}^T\mathbf{E}\mathbf{B}$$

where

$\mathbf{E}$ is the elasticity matrix,
$\mathbf{B} = \mathbf{D}\mathbf{N}$,
$\mathbf{D}$ is the differential operator,
$\mathbf{N}$ is the shape function matrix.

Matrix $\mathbf{B}$ consists of derivatives of shape functions of the element and does not depend on the material properties. $\mathbf{E}$ for isotropic materials is a function of the Young's modulus E and the Poisson's ratio ν. $\mathbf{E}$ for two-dimensional plane strain analysis can be written as:

$$\mathbf{E} = \frac{E}{(1+\nu)(1-2\nu)} \begin{bmatrix} 1-\nu & -\nu & 0 \\ -\nu & 1-\nu & 0 \\ 0 & 0 & \frac{1-2\nu}{2} \end{bmatrix}$$

The Young's modulus appears as a multiplying constant and can be extracted out as follows:

$$\mathbf{E} = E\mathbf{P}$$

where

$$\mathbf{P} = \frac{1}{(1+\nu)(1-2\nu)} \begin{bmatrix} 1-\nu & -\nu & 0 \\ -\nu & 1-\nu & 0 \\ 0 & 0 & \frac{1-2\nu}{2} \end{bmatrix}$$

Equation 1, used to determine the unknown displacements, can be rewritten as

$$\mathbf{B}_{aa}^{T}\mathbf{P}_{aa}\mathbf{B}_{aa}\mathbf{U}_{a} = -\mathbf{B}_{ab}^{T}\mathbf{P}_{ab}\mathbf{B}_{ab}\mathbf{U}_{b}$$

It can be seen that, as $\mathbf{P}$ depends only on ν and $\mathbf{B}$ is a function of the element shape functions, the above equation is independent of E, the Young's modulus. Hence, displacements and strains in a uniform plane strain finite element model with prescribed displacements and no prescribed forces are independent of the Young's modulus. Stresses are dependent on the Young's modulus, as they are obtained by multiplying strains by the elasticity matrix $\mathbf{E}$ which depends on E.

References

Boussinesq, J., 1985, *Application des Potentials á l'Etude de l'Equilibre et du mouvement des Solides Elastiques* Gauthier-Villars, Paris.

Cook, T. H., 1975, "The Mechanical Characterization of Human Skin In Vivo," PhD thesis, Stevens Institute of Technology, Castle Point, Hoboken, NJ.

Danielson, D A., 1984, "Human Skin as an Elastic Membrane," *J. Biomechanics,* Vol. 6, pp. 539–546, 1973.

Darian-Smith, I., "The Sense of Touch· Performance and Peripheral Neural Processes," *Handbook of Physiology - The Nervous System—III,* pp. 739–788

Fung, Y. C., 1981, *Biomechanics* Springer, New York.

Grigg, P. and Hoffman, A. H., 1984, 'Ruffini Mechanoreceptor in Isolated Joint Capsule: Responses Correlated with Strain Energy Density," *Somatosensory Research,* Vol. 2, No. 2, pp. 149–162

Johansson, R. S and Vallbo, A B., 1983, "Tactile Sensory Coding in the Glabrous Skin of the Human Hand," *Trends in Neuroscience,* Vol. 6, pp. 27–32

Lanir, Y., 1987, "Skin Mechanics," *Handbook of Bioengineering,* chapter 11, McGraw-Hill, pp 11 1–11 25.

Lanir, Y., Dikstein, S., Hartzshtark, A., and Manny, V., 1990, "In Vivo Indentation of Human Skin," *J. of Biomechanics,* Vol 112, pp 63–69.

Lighthill, J., 1991, "Biomechanics of Hearing Sensitivity," *Journal of Vibration and Acoustics,* Vol. 113, pp. 1–13

Phillips, J. R., and Johnson, K O., 1981a, "Tactile Spatial Resolution—II. Neural Representation of Bars, Edges and Gratings in Monkey Afferents," *J. Neurophysiol.,* Vol. 46, No. 6, pp 1192–1203.

Phillips, J. R., and Johnson, K O., 1981b, "Tactile Spatial Resolution—III A Continuum Mechanics Model of Skin Predicting Mechanoreceptor Responses to Bars, Edges, and Gratings," *J Neurophysiol,* Vol. 46, No. 6, pp. 1204–1225.

Srinivasan, M. A., 1989, "Surface Deflection of Primate Fingertip Under Line Load," *J. Biomechanics,* Vol. 22, No 4, pp 343–349.

Srinivasan, M. A., Gulati, R J., and Dandekar, K., 1992, "In Vivo Compressibility of the Human Fingerpad," *Advances in Bioengineering,* Vol. 22, pp. 573–576.

Sussman, T., and Bathe, K.-J., 1987, "A Finite Element Formulation for Nonlinear Incompressible Elastic and Inelastic Analysis," *J Computers and Structures,* Vol. 26, No. 1/2, pp 357–409.

Thacker, J. G., 1976, "The Elastic Properties of Human Skin In Vivo," PhD thesis, University of Virginia, Jan

Timoshenko, S. P., and Goodier, J. N., 1982, *Theory of Elasticity* McGraw-Hill, New York.

Ugural, A. C., and Fenster, S. K., 1981, *Advanced Strength and Applied Elasticity: The SI Version,* chapter 2, Elsevier, pp. 49–50.